Int. J. Electrochem. Sci., 13 **(2018)** 9888 – 9904, doi: 10.20964/2018.10.31

International Journal of
ELECTROCHEMICAL
SCIENCE
www.electrochemsci.org

Inhibitory Effect of *Pinus massoniana* Needle Extract on Corrosion of Q235 Steel in Hydrochloric Acid Medium

Xia Wang[*], *Shuai-fei Ren, Dai-xiong Zhang, Huan Jiang, Yue Gu*

School of Material Science and Engineering, Southwest Petroleum University, Chengdu Sichuan 610500, China
[*]E-mail: duh1478@163.com

Received: 25 May 2018 / *Accepted:* 11 July 2018 / *Published:* 1 September 2018

An extract of *Pinus massoniana* needles(PMNE) was obtained by soaking. The inhibitory effect of PMNE on the corrosion of Q235 carbon steel in 1 mol·L^{-1} HCl was investigated by the weight loss method, potentiodynamic polarization curves, electrochemical impedance spectroscopy and a quantum chemical study. The results indicated that PMNE was an efficient inhibitor with a corrosion inhibition efficiency of 95%. The equilibrium constant, free energy of adsorption, adsorption enthalpy were calculated and discussed. Thermodynamic analysis revealed that the adsorption of effective inhibitory constituents of PMNE on the Q235 steel surface was in accordance with the Langmuir isotherm equation, and was classed as physical adsorption. Polarization curves, and electrochemical impedance spectroscopy demonstrated that the corrosion inhibitor was a mixed inhibitor. A protective film of PMNE on the Q235 steel surface was investigated using scanning electron microscopy. Quantum chemical parameters were determined within the framework of the density functional theory .

Keywords: Pinus massoniana needle; plant-derived corrosion inhibitor; Q235 steel; electrochemical impedance spectroscopy; quantum chemical parameter

1. INTRODUCTION

Hydrochloric acid is employed in the pickling of metals, acid treatment of oil wells and descaling. Q235 steel is widely used in boiler plants, and gas and oil fields, and it is important to improve its resistance to corrosion[1]. As a convenient agents, corrosion inhibitors have great potential in the protection of metals. Therefore, as non-toxic, harmless inhibitors, plant-derived natural inhibitors are seen as ideal alternatives[2].

Pinus massoniana needles are among the main byproducts of the cultivation of this species of pine, which is characterized by its rapid regeneration, wide distribution and sustainable utilization of natural regenerated resources[3].The extract of PMNE contains nitrogen and oxygen compounds such

as, carbonyl compounds, as well as, aromatic compounds containing, for example, benzene rings and other groups. Its main constituents are arginine, shikimic acid, and caryophyllene as shown in Fig.1[4-9]. However, there have been few reports on the use of a pine needle extract as a corrosion inhibitor. Needles of the Huashan pine (*P.armandii*) have been declared to have a corrosion inhibiting effect on cold-rolled steel in H_2SO_4, and the highest corrosion inhibition efficiency recorded was 84%[10].This study aimed to investigate *P. massoniana* needles as a natural corrosion inhibitor for Q235 mild steel in a 1 mol·L^{-1} HCl solution.

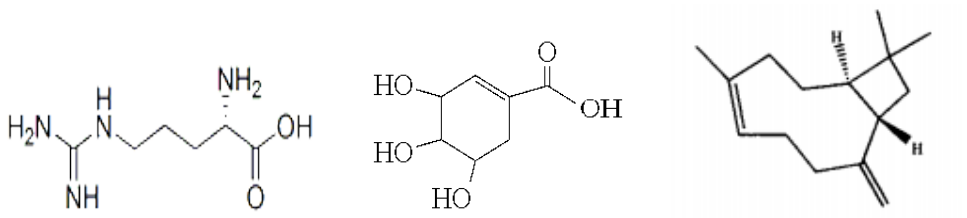

Arginine Shikimic acid caryophyllene

Figure 1. Structure of the active constituents of PMNE.

2. EXPERIMENTAL

2.1 Materials

Q235 steel coupons with the following composition (wt.%) were used: C 0.12%, Mn 0.36%,Si 0.15%,P 0.017%,S 0.013%,Ni 0.01%,Cr 0.01% and the balance Fe. *P. massoniana* needles were purchased, washed and dried, heated at 80 ℃ for 48h for drying, crushed, and then screened with a 500 mesh sieve, and the powder was placed in a cone-shaped bottle for used. A sample of 10g *P. massoniana* pine needle powder was immersed in 500mL of a 70% (volume fraction) ethanol solution, and soaked at a constant temperature of 70 ℃ for 3h, and the residue was removed by vacuum filtration. The extracted solution was then filtered and concentrated until the water and ethanol in the extract evaporated to obtain PMNE.

2.2 Fourier transform infrared spectroscopy (FTIR)

A Nicolet 6700 Fourier transform infrared spectrometer (ThermoElectron Corporation, USA)was utilized to analyze the molecular structures and chemical bonds of the substances present in the extract. The wave number range that was selectred was 4000-500cm $^{-1}$, the resolution is better than 0.1cm^{-1} and the signal-to-noise ratio was 4.5×10^5:1. Because PMNE is a liquid, KBr was ground into a powder and pressed for 5min at 15MPa to obtain a KBr pellet. Then PMNE was coated on the surface of the KBr pellet, which was placed in the infrared spectrometer.

2.3 Weight loss measurements

According to the ASTM G1-03 standard (2017), steel plate the test samples (30 mm x 15 mm x 3 mm) were employed for weight loss measurements. Three parallel samples of Q235 steels were abraded with a series of emery papers (200#, 400#, 600#, and 800#) and then washed with anhydrous ethanol and acetone, and blown with air. All the test sample were precisely weighed with an analytical balance (accuracy of 0.1 mg), and then placed into a closed three-necked flask. Then 300 mL of a 1 mol·L^{-1} HCl solution (pH = 0.1) was added, with the addition of PMNE at concentration of 0 g·L^{-1} (blank) , 0.2 g·L^{-1}, 0.4 g·L^{-1}, 0.6 g·L^{-1}, and 0.8 g·L^{-1}.The temperature was set at various values 25 ℃, 40 ℃, 55 ℃, and 70 ℃, and the samples were allowed to soak 4h. Then the surface corrosion products were cleaned, and the samples were rinsed with distilled water, and weighed exactly. The average corrosion rate (g · m^{-2} · h^{-1}) was calculated as shown in equation (1)[11]:

$$V_{corr} = \frac{W_0 - W_1}{s \times t} \qquad (1)$$

where V_{corr} is the corrosion rate, W_0 is the pre-corrosion weight of Q235 steel, W_1 is the weight of Q235 steel after corrosion, s is the exposed surface area (m^2), and t is the exposure time (h). The corrosion inhibition efficiency was calculated as shown in equation (2):

$$\eta\% = \frac{V_{corr}^0 - V_{corr}^{inh}}{V_{corr}^0} \times 100\% \qquad (2)$$

where ($\eta\%$) is the corrosion inhibition efficiency, V_{corr}^{inh} is the corrosion rate in the presence of the inhibitor, and V_{corr}^0 is the corrosion rate in the absence of the inhibitor.

2.4 Electrochemical measurements

The electrochemical workstation used was a Wuhan Correst Instruments CS310 model. Electrochemical experiments were carried out in a conventional three-electrode cell at 25 ℃, with a platinum counter electrode, a saturated calomel electrode coupled to a fine Luggin capillary as the reference electrode, and a Q235 steel working electrode [12]. In the experiments, Q235 steel (30 mm x 15 mm x 3 mm) was abraded with a series of emery papers (200#, 400#, 600#, and 800#) and then washed with anhydrous ethanol and acetone, and dried under a cold airstream. The test surface area of the WE was 1.0 cm ×1.0 cm, the other surfaces were covered with epoxy resin. The WE was immersed in the test solution for 60 min to establish a steady state open-circuit potential. After electrochemical impedance measurements, anodic and cathodic polarization curves were obtained at a scan rate of 0.5 mV· s^{-1} in the anodic and cathodic directions, respectively ($E = E_{corr} \pm 250\ mV$, where *Ecorr* is the corrosion potential). The relevant parameters were fitted using CView 2 software [13].The corrosion current I_{corr} and $I_{corr(inh)}$ and E_{corr} were determined by the Tafel extrapolation method. The corrosion inhibition efficiency was calculated using equation (3):

$$\eta\% = \frac{I_{corr} - I_{corr(inh)}}{I_{corr}} \times 100\% \qquad (3)$$

where I_{corr} and $I_{corr(inh)}$ are the corrosion current density in the absence and presence, respectively.

All experiments were performed in the frequency range from 100 mHz to 10 kHz with a peak-to-peak A.C. amplitude of 10 mV. EIS experiments were conducted using a computer controlled by

ZSimpWin3.10 software for fitting values of the charge transfer resistance (R_{ct}) and constant phase element (CPE). The corrosion inhibition efficiency was calculated using equation(4):

$$\eta\% = \frac{R_{ct}^{i} - R_{ct}^{0}}{R_{ct}^{i}} \times 100\% \qquad (4)$$

where R_{ct}^{0} and R_{ct}^{i} are the charge transfer resistance in the absence and presence, respectively, of the inhibitor.

2.5 Surface analysis

Q235 steel samples were abraded with a series of emery papers (200#, 400#, 600#, and 800#) and then washed with anhydrous ethanol and acetone, and dried. The surface morphologies of samples exposed to the 1 mol·L^{-1} HCl solution with different concentrations of PMNE were studied using a scanning electron microscope (Zeiss EVO/MA15). The analysis by scanning electron microscopy was carried out after all samples were immersed for 6 h at 25 ℃.

2.6 Theoretical calculation procedure

Molecular sketches of arginine, shikimic acid, and caryophyllene were drawn using the GaussView 5.0 visualization program. All quantum computations were performed using the Gaussian 09W software package at the B3LYP/6-31G(d,p) level of theory by a density functional theory method. The B3LYP/6-31G(d,p) functional has been widely used to study the relationship between the inhibition efficiency of a molecule and its electronic properties[14,15]. We studied calculated properties such as the total energy, dipole moment, highes occupied molecular orbital (HOMO), lowest unoccupied molecular orbital (LUMO), and band gap to determine the corrosion efficiency of arginine, shikimic acid and caryophyllene.

3. RESULTS

3.1 Infrared spectroscopy characterization

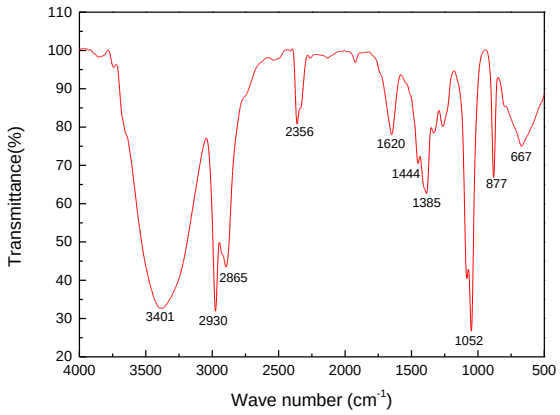

Figure 2. FTIR spectrum of PMNE

The FTIR spectrum of PMNE is shown in Fig. 2, and the corresponding functional groups are listed in Table 1. Among the FTIR peaks, the strong absorption band at 3401 cm^{-1} is due to the superposition of the three stretching vibration peaks of –COOH, O–H, and N–H groups. The absorption peak near 2930 cm^{-1} is due to asymmetric stretching vibrations of methylene groups. A band due to N–H deformation can be seen at 2865 cm^{-1}. The absorption peak at 2356 cm^{-1} is due to C=C stretching vibrations[16,17], whereas the absorption peak at 1620 cm^{-1} is due to C=O stretching vibrations. Peaks corresponding to the stretching and bending modes of $–CH_3$ groups were observed at 1385 cm^{-1}. The absorption peak at 1052 cm^{-1} was assigned to C–N stretching, whereas the peaks in the wavenumber regions of 1444 cm^{-1}, 877 cm^{-1}, and 667 cm^{-1} were assigned to the stretching modes of aliphatic and aromatic C–H groups[18,19].

The FTIR results indicate that PMNE contains substances such as volatile oils, sterols, and flavonoids. It also possesses nitrogen- and oxygen-containing functional groups (C=O, N–H, O–H, C–O, C–H, C–N, etc.). Plant-derived corrosion inhibitors generally possess polar groups containing oxygen, nitrogen, and sulfur atoms and nonpolar groups comprising hydrocarbon chains. The former are hydrophilic and endow the inhibitor molecule with a certain degree of solubility. It can be firmly adsorbed on a metal surface and form a thin film to protect the metal[20]. The latter are hydrophobic and form a hydrophobic film on a metal surface, which prevents corrosive ions from approaching the metal surface. Thus, the extracted PMNE has great potential in applications as a corrosion inhibitor.

Table 1. Results of FTIR analysis of PMNE

Absorption peaks（cm^{-1}）	Functional groups	Spectral band attribution
3401	-COOH, O-H, N-H superposition	stretching
2930	$-CH_2$	stretching
2865	N-H	bending
2356	C=C	stretching
1620	C=O	stretching
1385	$-CH_3$	bending
1052	C-N	stretching
1444,877,667	C-H	stretching

3.2 Weight loss measurements

The influence of PMNE on the corrosion behavior of Q235 steel in a 1 mol L^{-1} HCl solution as determined by weight loss measurements is illustrated in Fig. 3. At 25 °C with an inhibitor concentration of 0.8·g L^{-1}, the corrosion rate of Q235 steel was 3.6 $g·m^{-2}·h^{-1}$, which indicates an excellent inhibition efficiency of 95% by comparison with the corrosion rate of 79.9 $g·m^{-2}·h^{-1}$ in the absence of the inhibitor. With an increase in the solution temperature, the corrosion inhibition efficiency decreased. This phenomenon may be attributed to the higher corrosion rate and more vigorous evolution of hydrogen at higher temperatures. Corrosion inhibitors are difficult to adsorb on

the surface of Q235 steel. At the same temperature, the inhibition efficiency increased with an increase in the inhibitor concentration, which shows that more inhibitor molecules were adsorbed on the Q235 steel surface, which slowed down the corrosion process.

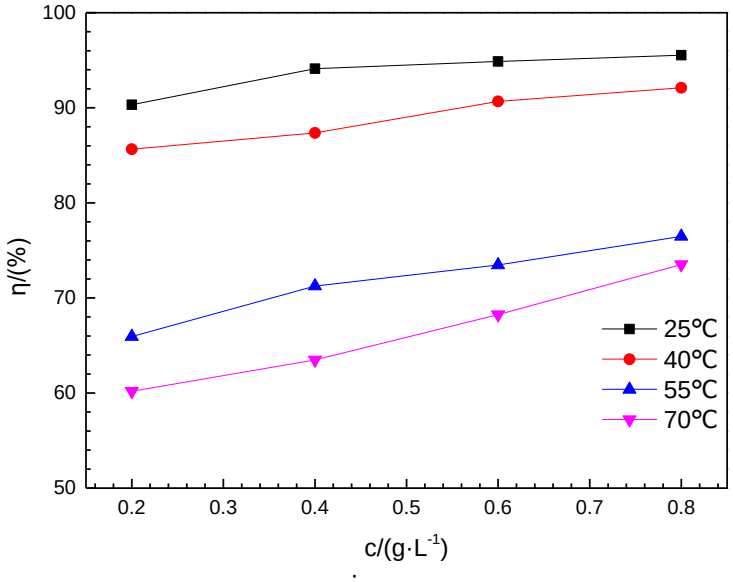

Figure 3. Corrosion inhibition efficiency at different temperatures and concentrations

3.3 Electrochemical experiments

3.3.1 Potentiodynamic polarisation curves test

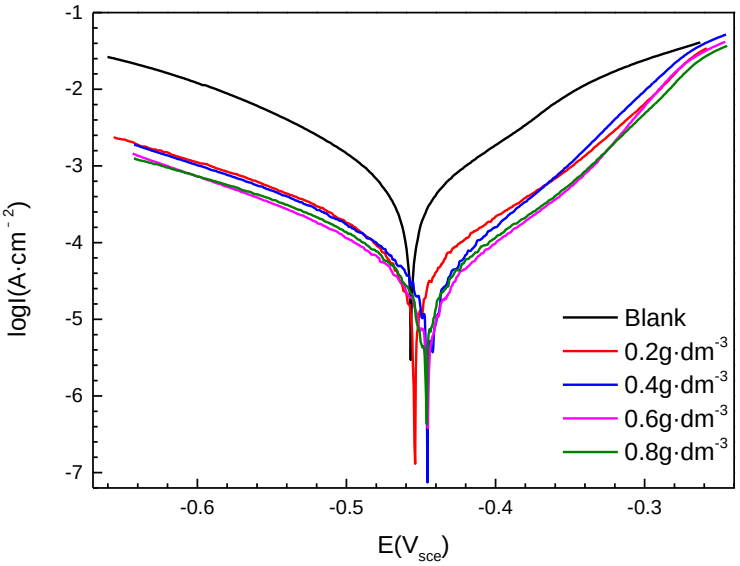

Figure 4. Polarization curves for different concentrations of the PMNE inhibitor at 25 °C

The influence of PMNE on the corrosion behavior of Q235 steel in a 1 mol· L^{-1} HCl solution as determined by recording potentiodynamic polarization curves is illustrated in Fig. 4. It can be observed that the cathodic reaction was highly inhibited, which is evident from the decrease in the corrosion current. However, the anodic reaction was slightly inhibited, as revealed by the anodic arms of the curves. Moreover, the inhibition efficiency increased with the inhibitor concentration. The results indicate that PMNE was a mixed inhibitor in the experimental temperature range. Mourya et al.[21] reported that *Tagetes erecta* extract (TEE) acted as a mixed inhibitor of the corrosion of mild steel in H_2SO_4, as demonstrated by potentiodynamic polarization parameters. The potentiodynamic polarization behavior of TEE corresponds to that of PMNE, and the cathodic curves were clearly shifted toward a lower current density with the addition of TEE or PMNE.

Electrochemical kinetic parameters, namely, E_{corr}, I_{corr}, the anodic Tafel slope (β_a), and the cathodic Tafel slope (β_c), were obtained using CView 2 software, as shown in Table 2

Table 2. Polarization parameters for Q235 steel in 1 mol· L^{-1} HCl in the absence and presence of different concentrations of PMNE at 25 °C

Concentration g/L	**$-E_{corr}$ mV**	**I_{corr} μA cm^{-2}**	**β_a mV/decade**	**$-\beta_c$ mV/decade**	**η %**
blank	457	556	93	102	-
0.2	445	51	73	102	88%
0.4	446	34	62	95	93%
0.6	451	29	79	100	94%
0.8	444	22	64	93	96%

Table 2 gives the results for the electrochemical kinetic parameters; no fundamental change in E_{corr} occurred when the concentration of the PMNE inhibitor was increased. The value of I_{corr} decreased gradually from 556 μA cm^{-2} to 22 μA cm^{-2}, which implies a significant decrease in the corrosion rate. The E_{corr} values were all less than 85 mV[21,22], which indicates that PMNE was a mixed inhibitor. The corrosion inhibition efficiency increased with an increase in the concentration of the PMNE inhibitor and was as high as 96% when the PMNE concentration was 0.8 g· L^{-1}

3.3.2 Electrochemical impedance spectroscopy

The influence of increasing concentrations of the PMNE inhibitor on the corrosion behavior of Q235 steel in a 1 mol· L^{-1} HCl solution measured in terms of the impedance response is given in Fig. 5. Nyquist plots (Fig. 5a) are characterized by a depressed capacitive semicircle, which should be attributed to the heterogeneity of the electrode surface and the double-layer capacitance (C_{dl})[23]. The impedance spectra are not perfect semicircles but are depressed with their centers beneath the real axis

and resemble depressed capacitive loops. This phenomenon often corresponds to surface heterogeneity. With an increase in the inhibitor concentration the radius of the capacitive arc increased significantly but the shape of the arc was roughly the same, which indicates that the corrosion mechanism was unchanged. The corrosion resistance of an electrode can be represented by the impedance mode |Z| at low frequencies. The higher is the value of |Z|, the better is the inhibitory effect. As shown in Fig. 5b, the value of |Z| increased significantly after the addition of the corrosion inhibitor. Phase angle plots (Fig. 5c) showed that after the addition of the corrosion inhibitor the phase angle increased, which indicated that the corrosion-inhibiting effect was greater.

The equivalent circuit shown in Fig. 6 was selected to determine the values of C_{dl} and R_{ct}[24].

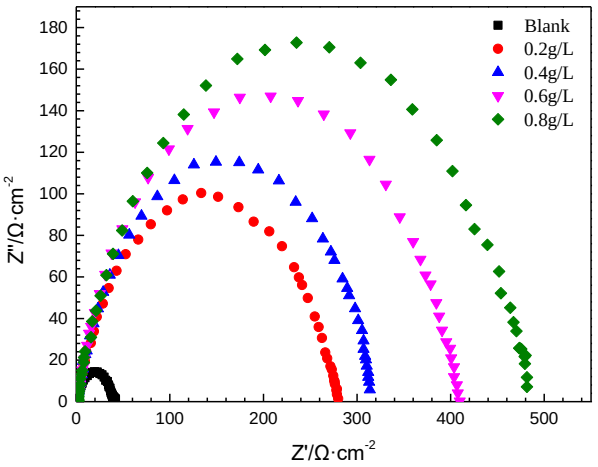

(a)Nyquist plots

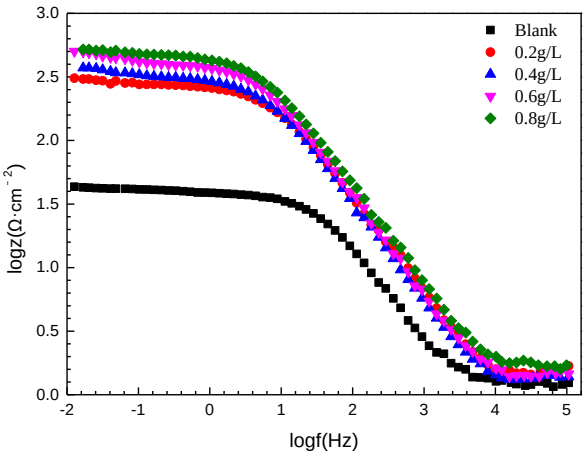

(b)Bode plots

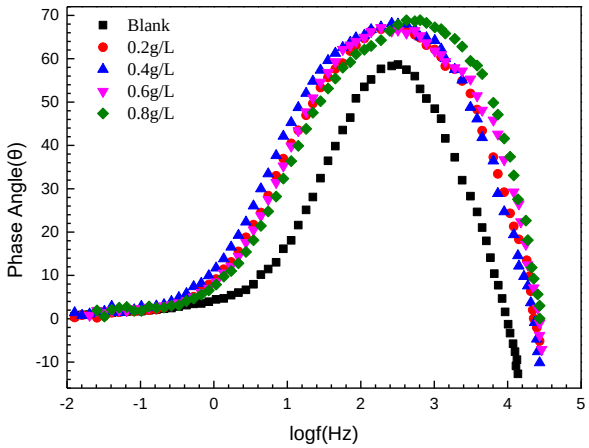

(c)Phase angle plots

Figure 5. Nyquist spectra of Q235 steel in the presence of the PMNE corrosion inhibitor with different concentrations at 25 °C: (a) Nyquist plots, (b) Bode plots, and (c) phase angle plots.

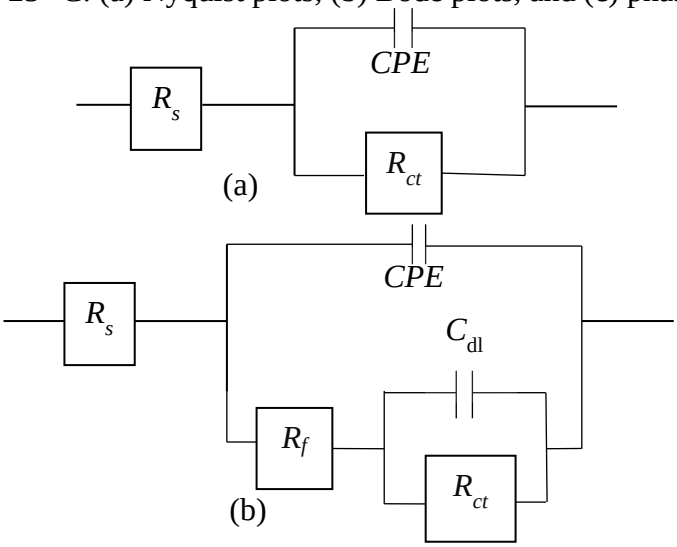

Figure 6. Equivalent circuit diagrams of (a) a blank sample and (b) a sample treated with PMNE. R_s is the solution resistance, R_{ct} is the charge transfer resistance, and R_f is the membrane resistance.

Parameters calculated from EIS are listed in Table 3. The inhibition efficiency (η) was also calculated using equation (4). The admittance (Y_{CPE}) can be calculated as follows:

$$Y_{CPE} = Y_0 (j\omega)^n \qquad (5)$$

where Y_0 is the amplitude comparable to a capacitance, j is the square root of −1, ω is the angular frequency ($\omega = 2\pi f_{max}$) at which the imaginary part of the impedance ($-Z_{im}$) is a maximum, where f_{max} is the corresponding AC frequency, and n is the phase shift, which can be used as an indicator of the heterogeneity or roughness of the Q235 steel surface[25].

Table 3. Electrochemical impedance parameters for Q235 steel in a 1 mol· L^{-1} HCl solution in the absence and presence of PMNE at 25 °C.

Concentration g/L	C_{dl} /μFcm^{-2}	n	R_{ct} /Ω·cm^2	η %
blank	114	0.85	31	-
0.2	55	0.83	279	88
0.4	63	0.82	334	90
0.6	59	0.83	430	92
0.8	46	0.81	478	93

The value of C_{dl} can be calculated by incorporating the values of the CPE parameters Y and n in equation (6)[26]:

$$C_{dl} = \frac{Y\omega^{n-1}}{\sin(n(\pi/2))} \qquad (6)$$

Table 3 shows that the R_{ct} value increases with the concentration of the PMNE inhibitor. This indicates an increase in resistance to ionization of the metal and a decrease in the corrosion rate of the metal. This can be attributed to the adsorption of PMNE and can be explained by the formation of a protective film of PMNE at the metal/solution interface[27]. In addition, Hu et al.[24] discussed the adsorption of an inhibitor based on a *Capsella bursa-pastoris* extract at a Q235 steel/HCl solution interface in preference to H_2O molecules, so that the R_{ct} value increased and the C_{dl} value decreased. However, they did not discuss the causes of the reduction in the C_{dl} value. The value of C_{dl} decreased (Table 3) with the addition of PMNE, which was probably due to a decrease in the local dielectric constant and suggested that PMNE was adsorbed over the Q235 steel surface.

4. DISCUSSION

4.1. Adsorption

The mechanism of action of the inhibitor can be described by an adsorption isotherm. It is assumed that the adsorption of PMNE inhibitor molecules on the Q235 steel surface conforms to the Langmuir adsorption isotherm[28,29]:

$$C/\theta = 1/K_{ads} + C \qquad (7)$$

where θ is the surface coverage, which is expressed by the ratio η_w%/100, C is the concentration of the inhibitor, and K_{ads} is the equilibrium adsorption constant. Linear regression between C/θ and C was performed, as shown in Fig. 7, and the parameters are listed in Table 4.

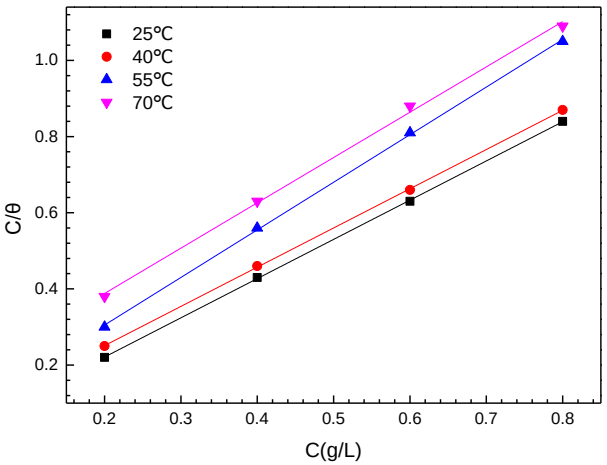

Figure 7. Langmuir adsorption isotherm model for Q235 steel in the presence of the PMNE inhibitor at different concentrations.

Table 4. Langmuir parameters for Q235 steel in a 1 mol· L^{-1} HCl solution in the presence of different PMNE concentrations and at different temperatures.

Temperature（℃	Slope	K_{ads} (L/g)	R^2
25	1.0	66.7	0.9
40	1.0	22.2	0.9
55	1.1	18.2	0.9
70	1.0	6.7	0.9

Figure 7 and Table 4 demonstrate that the slope of a plot of C/θ against C for PMNE is nearly 1, and the regression correlation coefficient is high (0.99) at different temperatures. It is suggested that the adsorption of PMNE molecules on the Q235 steel surface followed the Langmuir isotherm[30,31]. Rocha[34] investigated the inhibition efficiency of aqueous extracts of fruit peels, and their adsorption behavior followed the Langmuir model. However, there are no relevant effective corrosion inhibitors that comprise extracts of fruit peels. The corrosion inhibitor was adsorbed as a single molecular layer on the Q235 steel surface, which would effectively inhibit corrosion by HCl. The equilibrium adsorption constants (K) at 25 °C and 70 °C were 66.67 L g^{-1} (K_1) and 6.67 L g^{-1} (K_4), respectively. The lower K value at the higher temperature indicates that when the temperature increased the equilibrium adsorption constant decreased accordingly, which would lead to a decrease in the adsorption capacity for the PMNE inhibitor. Therefore, the corrosion inhibitor molecules were more likely to be desorbed from the surface of Q235 steel.

4.2. Thermodynamic and kinetic parameters

The value of K_{ads} can be calculated from the intercept of the straight line in Fig. 7, as shown in Table 4. The free energy of adsorption (ΔG_{ads}) was calculated from equation (8):

$$\Delta G_{ads} = -RTln(55.5 \times K_{ads}) \quad (8)$$

where R is the gas constant (8.314 J mol^{-1} $\cdot K^{-1}$), T is the absolute temperature (K), and 55.5 is the molarity of water. In order to investigate the adsorption of inhibitor molecules, the adsorption enthalpy (ΔH_{ads}) and adsorption entropy (ΔS_{ads}) were calculated using the van't Hoff equation:

$$lnK_{ads} = -\frac{\Delta H_{ads}}{RT} + \frac{\Delta S_{ads}}{R} + ln55.5 \quad (9)$$

A plot of ln K_{ads} against 1000/T for Q235 steel in 1 mol· L^{-1} HCl in the presence of PMNE is shown in Fig. 8. After linear fitting, the slope of the line is $-\Delta H_{ads}/R$, and the value of ΔH_{ads} represents the standard adsorption enthalpy. The standard adsorption entropy can be determined by the following basic thermodynamic equation:

$$\Delta S_{ads} = \frac{\Delta H_{ads} - \Delta G_{ads}}{T} \quad (10)$$

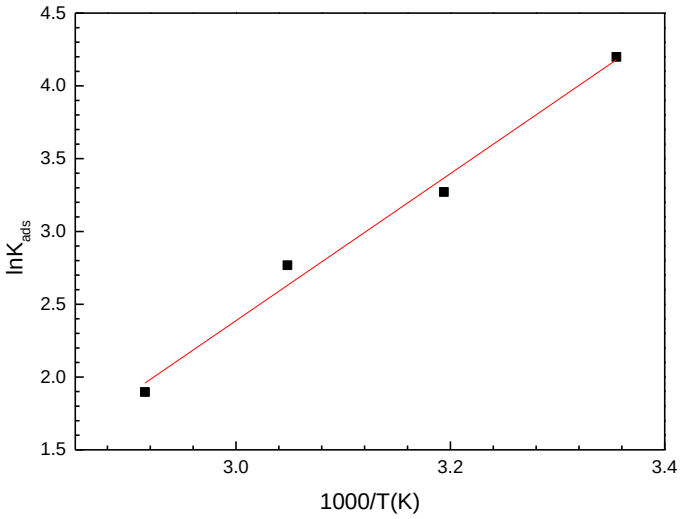

Figure 8. Plot of ln K_{ads} versus 1000/T for the interface between Q235 steel and the PMNE corrosion inhibitor.

Table 5. Thermodynamic parameters of adsorption of PMNE

Temperature (K)	ΔG_{ads} (KJ mol^{-1})	ΔH_{ads} (KJ mol^{-1})	ΔS_{ads} (J mol^{-1} K^{-1})
298	- 19.9	- 41.9	- 73.8
313	- 18.5	- 41.9	- 74.9
328	- 18.8	- 41.9	- 70.4
343	- 16.8	- 41.9	- 73.2

From the data in Table 5, the adsorption of PMNE on the Q235 steel surface is classed as physical adsorption. The results for the relationship between the temperature and corrosion inhibition efficiency measured via the weight loss method show that the corrosion inhibition efficiency decreased as the temperature of the corrosion medium increased. The negative value of ΔH_{ads} shows that the

adsorption of the PMNE inhibitor was an exothermic process and indicates that a rise in temperature was not conducive to the adsorption of inhibitor molecules. At different temperatures $\Delta G_{ads} < 0$, which indicates that the adsorption process of PMNE molecules on the Q235 steel surface was spontaneous. The calculated values of ΔG_{ads} were approximately −20 kJ mol^{-1}, which indicates that the adsorption mechanism of PMNE in a 1 mol L^{-1} HCl solution at the studied temperatures was physisorption[32]. From Table 5, the value of ΔG_{ads} ranged from −19.9 kJ mol^{-1} to −16.8 kJ mol^{-1} at different temperatures, which effectively confirms that the mechanism of adsorption of PMNE on the Q235 steel surface was physical. Likewise, $\Delta S_{ads} < 0$, which shows that the process of adsorption of corrosion inhibitor molecules on the Q235 steel surface was exothermic.

4.3. Scanning electron microscopy

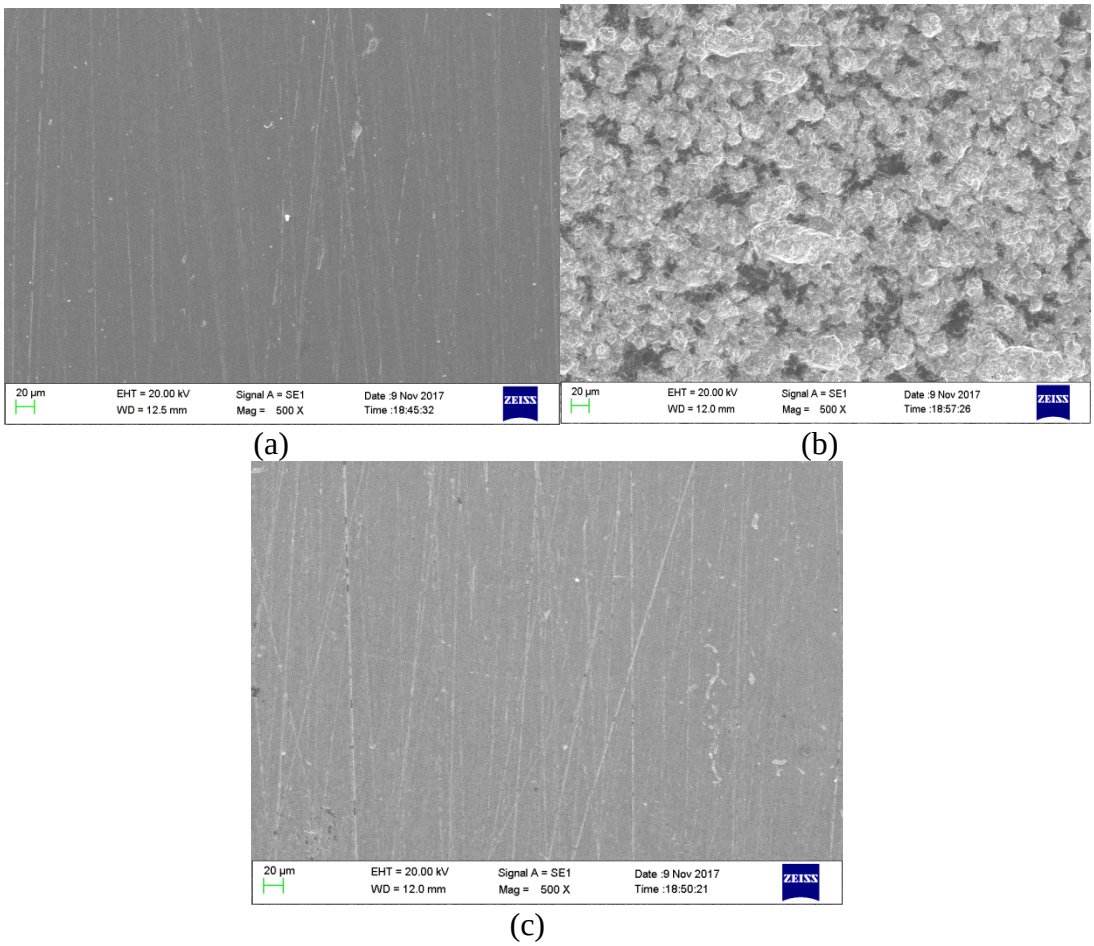

Figure 9. Scanning electron micrographs of Q235 steel (a) before and (b) after immersion in 1 mol·L^{-1} HCl and (c) after immersion in 1 mol ·L^{-1} HCl with 0.2 g ·L^{-1} PMNE at 25 °C for 6 h.

Figure 9a shows that the surface of Q235 steel was smooth before being immersed in 1 mol·L^{-1} HCl. Figure 9b indicates characteristic features of the corrosion of carbon steel in an acid in that the surface of the Q235 steel electrode was highly corroded, which was caused by direct attack by the strong acid[33]. Figure 9c shows visible scratches and a smoother surface than that in Fig. 9b. It can be

concluded that the inhibitor molecules can form complex compounds with metal ions, which can protect the metal surface from an acid solution.

4.4. Quantum Chemical Parameters

The fully optimized minimum-energy geometrical configurations of arginine, shikimic acid, and caryophyllene are shown in Fig. 10. Quantum chemical properties such as the total energy, energy of the HOMO (E_{HOMO}), energy of the LUMO (E_{LUMO}), energy gap (ΔE), dipole moment (μ), and number of transferred electrons (ΔN) are listed in Table 6. The value of ΔN was calculated using the following equation[34]:

$$\Delta N = \frac{\chi_{Fe} - \chi_{inh}}{2(\varepsilon_{Fe} + \varepsilon_{inh})} \qquad (11)$$

where χ_{Fe} and χ_{inh} denote the absolute electronegativity of iron and the inhibitor molecule, respectively, whereas ε_{Fe} and ε_{inh} denote the absolute hardness of iron and the inhibitor molecule, respectively. For iron atoms, the theoretical χ value of 7 eV mol^{-1} and the ε value of 0 eV mol^{-1} were used to calculate the fraction of electrons transferred, i.e., ΔN, from the inhibitor to the iron atom. Other quantities include the ionization potential (I), electron affinity (A), electronegativity (χ), global hardness (ε), and global softness (σ), as follows:

$$I = -E_{HOMO} \qquad (12)$$

$$A = -E_{LUMO} \qquad (13)$$

$$\Delta E = A - I \qquad (14)$$

$$\chi = \frac{I + A}{2} \qquad (15)$$

$$\varepsilon = \frac{I - A}{2} \qquad (16)$$

$$\sigma = \frac{1}{\eta} \qquad (17)$$

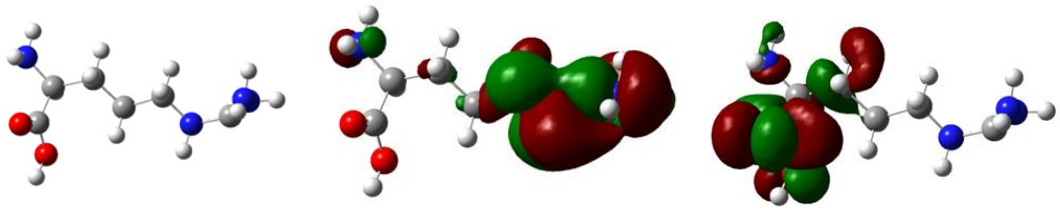

Arginine HOMO LUMO

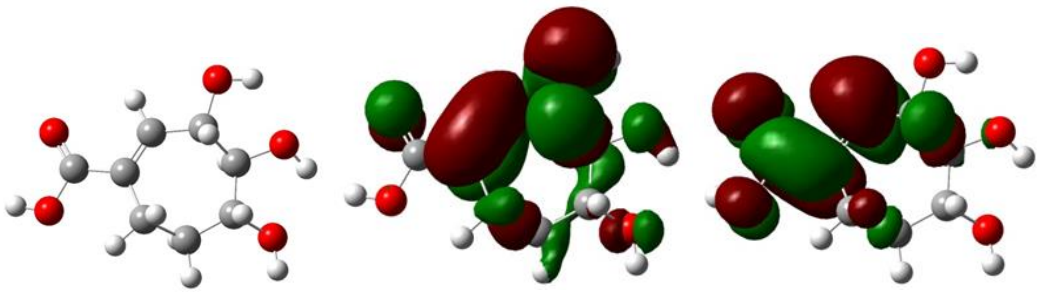

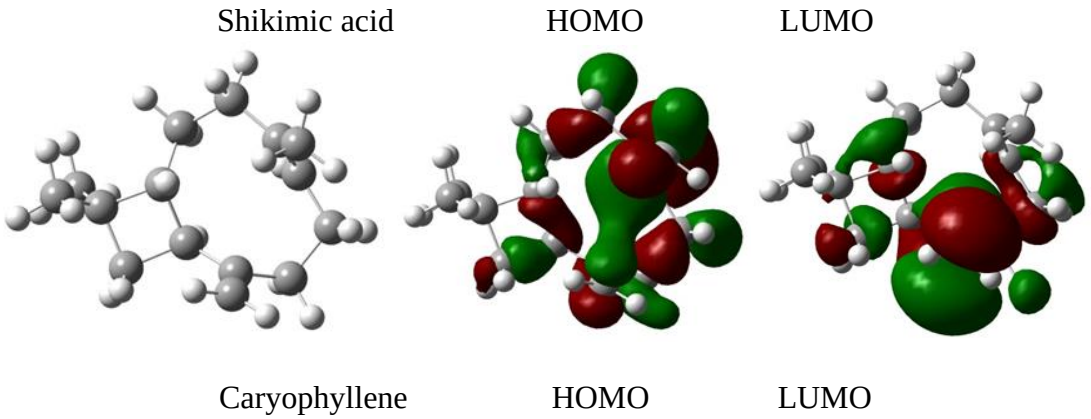

Figure 10. Optimized structures of arginine, shikimic acid, and caryophyllene and the HOMO and LUMO of the molecules.

Table 6. Computed quantum chemical parameters for arginine, shikimic acid, and caryophyllene at 25 °C.

Molecule	Total Energy (au)	E_{HOMO} (ev)	E_{LUMO} (ev)	μ (D)	ΔE (ev)	ε (ev)	σ (ev^{-1})	χ	ΔN
Arginine(Arg)	-607	-5.6	-0.3	1.6	5.2	2.6	0.3	2.9	0.8
Shikimic acid(Sa)	-688	-6.9	-1.5	5.6	5.3	2.7	0.4	4.3	0.5
Caryophyllene(Car)	-586	-5.9	0.5	0.4	5.4	3.2	0.3	2.7	0.6

Table 7. Comparison of effective corrosion-inhibiting groups in various plant-derived corrosion inhibitors.

Inhibitor	Inhibiting groups
TEE[21]	C=C, C-O,π-electrons
HPMC[22]	$-NH_2$,-COOH
VGOD,VGOH,VGOO,VGOL[25]	C=N, π-electrons
PCs[35]	N-H, C≡N, C-O
PSC[37]	C=N,N-H

From the HOMO and LUMO distribution maps in Fig. 10, it can be seen that the energy of the HOMO of arginine is mainly delocalized near the the N–H bonds on the alpha and side-chain N atoms in arginine, and the energy of the LUMO is mainly delocalized near the O–H bond and –COOH group. The energy of the HOMO of shikimic acid is mainly delocalized near the C=C and O–H bonds, and the energy of the LUMO is mainly delocalized near the C=O and C–C bonds. The energy of the HOMO of caryophyllene is mainly delocalized near the C=C and C–C bonds, and the energy of the LUMO is mainly delocalized near the $–CH_2$ groups. By comparison with Table 7, this shows that the effective inhibitor molecules are adsorbed on the surface of Q235 steel through these groups, which contain nitrogen and oxygen atoms, unsaturated bonds, and nonpolar hydrocarbon chains, to form a protective film and achieve a corrosion-inhibiting effect.

ΔE is an important indicator of molecular stability. The lower is the value of ΔE, the easier it is for the molecule to participate in chemical reactions. The values of ΔE are in the following order: arginine (5.2 eV) < shikimic acid (5.3 eV) < caryophyllene (5.4 eV); this shows that arginine molecules are more easily adsorbed on the metal surface to form a protective film. The value of ΔN shows the inhibitory effect that results from electron donation. According to a study by Lukovits[35], if the value of $\Delta N < 3.6$, the inhibition efficiency increases with an increase in the electron-donating ability of the inhibitor at the metal surface. In addition, it was observed [36] that the inhibition efficiency increased with an increase in the value of ΔN. The values of ΔN are in the following order: arginine (0.8) > caryophyllene (0.6) > shikimic acid (0.5); this shows that arginine may have higher inhibition efficiency than the other compounds.

5. CONCLUSIONS

(1) PMNE exhibited a strong corrosion-inhibiting effect on Q235 steel in 1 mol· L^{-1} HCl, and the corrosion efficiency increased with the PMNE concentration and decreased with the temperature.

(2) PMNE was an eco-friendly mixed inhibitor. At 25 °C, the corrosion inhibition efficiency was 96% for a concentration of 0.8 g· L^{-1}.

(3) The adsorption of PMNE on the Q235 steel surface in 1 mol· L^{-1} HCl obeyed the Langmuir adsorption isotherm model and was classed as physical adsorption.

(4) The negative signs of ΔG_{ads} and ΔH_{ads} indicated that the adsorption of PMNE on the Q235 steel surface in 1 mol· L^{-1} HCl was spontaneous and exothermic.

(5) The results of quantum chemical calculations provided complementary evidence that the active constituents of PMNE could achieve effective corrosion inhibition by means of groups containing nitrogen and oxygen atoms, unsaturated bonds, and nonpolar hydrocarbon chains.

References

1. M.A. Amin, S.S. El-Rehim, E.F. El-Sherbini and R.S. Bayoumi, *Electrochim. Acta*., 11(2007)3588.
2. S.H. Zaferani, M. Sharifi, D. Zaarei and M.R. Shishesaz, *J. Environ. Chem. Eng*., 4(2013)652.
3. Y.L. He, A.Q. Liu, M. Tigabu and P.F. Wu, *J. For. Res*., 2(2013)325.
4. J.W. Zhang, A.D. Rozario, J.M. Adams, X.Q. Liang, F.M.B. Jacques, T. Su and Z.K. Zhou. *Rev Palaeobot Palyno*., 215(2015)57.
5. F.W. Wang, F. Wang, X.L. Yang, Y.X. Bian and X. Jiang, *Environ. Sci. Res*., 31,(2010)503.
6. D.C. Wu, S. Li, D.Q. Yang and Y.Y. Cui, *Fitoterapia*., 82(2011)1202.
7. Y. Xu and H. Xiao, *Environ. Pollut*. , 221(2016)180.
8. C. Shen, W. Duan, B. Cen and J. Tan, *Sepu*., 24(2006)619.
9. L.H. Liu, L.S. Wang, D.D. Feng, F. Shen, Y.H. Zhou and X.M. Liu, *Chin. J. Anal. Lab*.,27 (2008) 75.
10. H. Fu, X.H. LI, S.R. Deng and M.Liu, *Corros. Mater. Prot*.,31(2010)160.
11. A.K. Satapathy, G. Gunasekaran, S.C. Sahoo, K. Amit and P.V. Rodrigues, *Corros. Sci*.,51(2009)2848.
12. X.H. Li, S.D. Deng, H. Fu and X.G. Xie, *Corros. Sci.*, 78(2014)29.
13. S. Ambrish, A. Ishtiaque and A. Mumtaz, *Arabian J. Chem.*, 9(2016)S1584.
14. B. Hirschorn, M.E. Orazem, B. Tribollet and M. Musiani, *J. Electrochem. Soc.*, 157(2010)C452.

15. B.M. Mistry, N.S. Patel, S. Sahoo and S. Jauharl, *Bull. Mater. Sci.*, 35(2012)459.
16. Y.A. Yang, D.Z. Wang and M.Z. Si, *J. Light .Sca.*, 4(2015)379.
17. S. Ambrish, Y.H. Lin, E. Ebenso, W.Y. Liu, J. Pan and B. Huang, *J. Ind. Eng. Chem.*, 24(2015) 219.
18. N.A. Odewunmi, S.A. Umoren and Z.M. Gasem, *J. Environ. Chem. Eng.*, 3(2015)286.
19. A. Okewale and A. Olaitan, *Int. J. Mater. Chem.*,7(2017)5.
20. K.P.V. Kumar, M.S.N. Pillai and G.R. Thusnavis, *J. Mater. Sci. Technol. (Sofia, Bulg.).*, 27(2011)1143.
21. P. Mourya, S. Banerjee and M.M. Singh, *Corros. Sci.*, 85(2014)352.
22. I.O. Arukalam, I.C. Madufor, O. Ogbobe and E.E. Oguzie, *Int. J. Appl. Sci. Eng. Res.*, 2(2013)613.
23. Q. Hu, Y. Qiu, G.A. Zhang and X.P. Guo, *Chin. J. Chem. Eng.*, 23(2015)1408.
24. N.A. Negma, N.G. Kandile, E.A. Badr and M.A. Mohammed, *Corros. Sci.*, 65(2012)94.
25. K. Jüttner. *Electrochim. Acta.*, 35(1990)1501.
26. B. Qian, J. Wang, M. Zheng and B. Hou, *Corros. Sci.*, 75(2013)184.
27. V. Sribharathy and S. Rajendran, *ISRN Corros*., 2013(12)265.
28. X. Li, S. Deng and H. Fu, *Corros. Sci.*, 62(2012)163.
29. V.V. Torres, R.S. Amado, C.D. Sá, T.P. Femandez, C.A. Riehl, A.G. Torres and E.D. Elia, *Corros. Sci.*, 53(2011)2385.
30. M. Lebrini, F. Robert, A. Lecante and C. Roos, *Corros. Sci.*, 53(2011)687.
31. K. Mallaiya, R. Subramaniam, S.S. Gowri, N. Rajasekaran and A. Selvaraj, *Electrochim. Acta.*, 56(2011)3857.
32. P. Muthukrishnan, P. Prakash, B. Jeyaprabha and K. Shankar, *Arabian J. Chem.*, 9(2015)1.
33. J.C.D. Rocha, J.A.C.P. Gomes and E. D'Elia, *Corros. Sci.*, 52(2010)2341.
34. K.R. Ansari, M.A. Quraishi and A. Singh, *J. Ind. Eng. Chem.*, 25(2015)89.
35. I. Lukovits, E. Kálmán and F. Zucchi, *Corrosion.*, 57(2001)3.
36. H. Ju, Z.P. Kai and Y. Li, *Corros. Sci.*, 50(2008)865.